Earth and Planetary Science Letters 513 (2019) 124–134

Contents lists available at ScienceDirect

Earth and Planetary Science Letters

www.elsevier.com/locate/epsl

The effect of core composition on iron isotope fractionation between planetary cores and mantles

Stephen M. Elardo [a,b,*], Anat Shahar [a], Timothy D. Mock [c], Corliss K. Sio [a,d]

[a] Geophysical Laboratory, Carnegie Institution of Washington, Washington, DC 20015, USA
[b] Department of Geological Sciences, University of Florida, Gainesville, FL 32611, USA
[c] Department of Terrestrial Magnetism, Carnegie Institution of Washington, Washington, DC 20015, USA
[d] Nuclear and Chemical Sciences Division, Lawrence Livermore National Laboratory, Livermore, CA 94550, USA

ARTICLE INFO

Article history:
Received 22 June 2018
Received in revised form 10 February 2019
Accepted 12 February 2019
Available online xxxx
Editor: F. Moynier

Keywords:
core formation
iron isotopes
experimental petrology
isotope geochemistry
mantle
planetary science

ABSTRACT

We have conducted high-pressure, high-temperature isotope exchange experiments between molten silicate and molten Fe–Si–C-alloys to constrain the effect of Si on equilibrium Fe isotope fractionation during planetary core formation. The values of $\Delta^{57}Fe_{Metal\text{-}Silicate}$ at 1850 °C and 1 GPa determined by high-resolution MC-ICP-MS in this study range from -0.013 ± 0.054‰ (2SE) to 0.072 ± 0.085‰ with 1.34–8.14 atom % Si in the alloy, respectively. These results, although not definitive on their own, are consistent with previous experimental results from our group and a model in which elements that substitute for Fe atoms in the alloy structure (i.e., Ni, S, and Si) induce a fractionation of Fe isotopes between molten silicate and molten Fe-alloys during planetary differentiation. Using *in situ* synchrotron X-ray diffraction data for molten Fe-rich alloys from the literature, we propose a model to explain this fractionation behavior in which impurity elements in Fe-alloys cause the nearest neighbor atomic distances to shorten, thereby stiffening metallic bonds and increasing the preference of the alloy for heavy Fe isotopes relative to the silicate melt. This fractionation results in the bulk silicate mantles of the smaller terrestrial planets and asteroids becoming isotopically light relative to chondrites, with an enrichment of heavy Fe isotopes in their cores, consistent with magmatic iron meteorite compositions. Our model predicts a bulk silicate mantle δ^{57}Fe ranging from −0.01‰ to −0.12‰ for the Moon, −0.06‰ to −0.33‰ for Mars, and −0.08‰ to −0.33‰ for Vesta. Independent estimates of the δ^{57}Fe of primitive mantle source regions that account for Fe isotope fractionation during partial melting agree well with these ranges for all three planetary bodies and suggest that Mars and Vesta have cores with impurity (i.e., Ni, S, Si) abundances near the low end of published ranges. Therefore, we favor a model in which core formation results in isotopically light bulk silicate mantles for the Moon, Mars, and Vesta. The processes of magma ocean crystallization, mantle partial melting, and fractional crystallization of mantle-derived melts are all likely to result in heavy Fe isotope enrichment in the melt phase, which can explain why basaltic samples from these planetary bodies have variable δ^{57}Fe values consistently heavier than our bulk mantle estimates. Additionally, we find no clear evidence that Fe isotopes were fractionated to a detectable level by volatile depletion processes during or after planetary accretion, although it cannot be ruled out.

1. Introduction

The ubiquity of Fe in the three major geochemical reservoirs in terrestrial planets – cores, mantles, and crusts – makes the Fe isotope system potentially powerful for understanding planetary differentiation. The Fe isotope compositions of planetary sample suites show significant variations relative to the narrow range found in chondrites, the average of which is $\delta^{57}Fe = \sim 0$‰ (relative to IRMM-014; Craddock and Dauphas, 2011), which implies that fractionations were produced by processes during and/or after planetary accretion. Magmatic iron meteorites almost ubiquitously have Fe isotope compositions that are heavy relative to chondrites, with δ^{57}Fe values ranging from close to chondritic up to 0.32‰ (Poitrasson et al., 2005; Williams et al., 2006). Although non-magmatic iron meteorites span a similar range in compositions, we do not consider them further as they are likely not the direct products of core formation, but rather other processes

* Corresponding author at: Department of Geological Sciences, University of Florida, Gainesville, FL 32611, USA.
E-mail address: selardo@ufl.edu (S.M. Elardo).

https://doi.org/10.1016/j.epsl.2019.02.025
0012-821X/

such as collisional heating. Interestingly, planetary silicate reservoirs span a similar range. Basaltic shergottites and non-cumulate eucrites, lavas from Mars and Vesta, respectively, both range from slightly negative to positive δ^{57}Fe values (Poitrasson et al., 2004; Weyer et al., 2005; Schoenberg and von Blanckenburg, 2006; Wang et al., 2012; Sossi et al., 2016a). Lunar basalts span a comparatively large range, from slightly negative values in volcanic glasses to very heavy values in high-Ti mare basalts (Poitrasson et al., 2004; Weyer et al., 2005). Terrestrial mantle xenoliths span a large range from roughly −0.8‰ to 0.2‰, in part due to the effects of metasomatism, alteration, and melt extraction (Weyer and Ionov, 2007; Zhao et al., 2010; Craddock et al., 2013; Poitrasson et al., 2013; Williams and Bizimis, 2014). However, a prominent peak in the global peridotite dataset close to the chondritic value provides evidence that Earth's upper mantle has a δ^{57}Fe near chondrites (see review by Dauphas et al., 2017). Mid-ocean ridge basalts (MORBs) are ubiquitously fractionated to fairly homogeneous δ^{57}Fe of ∼0.15‰, which is generally thought to be caused by partial melting (Williams et al., 2005; Weyer and Ionov, 2007; Craddock et al., 2013; Teng et al., 2013; Dauphas et al., 2014).

The differences in Fe isotope systematics between planetary samples have been attributed to various mechanisms. Crystal/liquid fractionation during fractional crystallization and mantle melting plays a role in generating the variability observed in lunar basalts, shergottites, and the abyssal peridotite-MORB offset (Weyer and Ionov, 2007; Craddock et al., 2013; Dauphas et al., 2014; Sossi et al., 2016a). However, the two fractionation mechanisms most frequently discussed are volatile depletion and core formation. The debate between these two mechanisms is largely a product of uncertainty regarding the δ^{57}Fe of bulk planetary mantles and the paucity of experimentally-determined fractionation factors between silicate minerals and melts, metallic melts, and vapors. There has been significant debate over whether core-mantle equilibration during planetary differentiation results in Fe isotope fractionation (Poitrasson et al., 2009; Hin et al., 2012; Shahar et al., 2015, 2016; Elardo and Shahar, 2017; Liu et al., 2017) and how important this effect is relative to other mechanisms (e.g., Poitrasson et al., 2004; Weyer et al., 2005; Schoenberg and von Blanckenburg, 2006; Poitrasson, 2007; Williams et al., 2012; Sossi et al., 2016a, 2016b). Our previous work has shown that Fe alloying with siderophile elements such as S and Ni results in Fe isotope fractionation during metal-silicate equilibration (Shahar et al., 2015; Elardo and Shahar, 2017), but a more complete picture of the compositional effects on and causes of this fractionation has been lacking. Here we present new experimental data on the effects of Si in planetary cores on Fe isotope fractionation between metal and silicate, and we examine (1) the cause of metal-silicate fractionation of Fe isotopes observed in the broader experimental literature from a metallic structure perspective, (2) the discrepancies in results between previous low-pressure experimental work (Poitrasson et al., 2009; Hin et al., 2012) and our own, and (3) the implications of this fractionation for the Fe isotope compositions of planetary mantles.

2. Experimental and analytical methods

2.1. Piston-cylinder experiments

Iron isotope exchange experiments were conducted at the Geophysical Laboratory (GL), Carnegie Institution of Washington. The silicate composition (Table 1) was the same ^{54}Fe spiked peridotite mix used by Elardo and Shahar (2017) and similar to that used by Shahar et al. (2015). Starting metal compositions were $Fe_{91}Si_9$ and $Fe_{95.5}Si_{4.5}$. Starting materials had a bulk Earth-like metal/silicate ratio (32 wt.% metal) with the exception of PC 1529, which had ∼20 wt.% metal. Experiments were conducted using a 1/2 inch diameter Boyd-England-style end-loaded piston cylinder. Experiments were run in talc-Pyrex cells with straight-walled graphite heaters at 1 GPa and 1850 °C. Inner parts were MgO with the exception of the thermocouple sheath, which was Al_2O_3. Stainless steel base plugs were enclosed by pyrophyllite sheaths. All MgO inner parts were dried at ∼900 °C for at least 1 h and were stored in a drying oven at ∼105 °C. Starting materials were loaded into high-purity graphite capsules and were stored in a desiccated drying oven at ∼105 °C typically for many days before use. Lead-foil and a MoS_2 suspension were used for lubrication within the pressure vessel. Experiments were pressurized cold to ∼1.25 GPa to promote a more complete compression of the cell prior to heating. Pressure was added as the cell compressed during heating to maintain the pressure of interest. Temperature was monitored with a type C ($W_5Re_{95}/W_{26}Re_{74}$) thermocouple. Experimental durations ranged between 0.5–3 h. Runs were quenched by cutting power to the assembly and cooled to ∼150 °C in ∼10–15 s.

2.2. Silicon drift detector–energy dispersive spectrometry (SDD–EDS)

A portion of each run product was mounted in epoxy and polished flat. The compositions of the silicate and metal phases were determined via SDD-EDS analyses using the JEOL 6500F field–emission scanning electron microscope at GL equipped with an Oxford X-Max 80 mm^2 Si drift detector. Although traditional EDS analysis is semi-quantitative at best, SDD-EDS analysis is equivalent to wavelength dispersive spectrometry analysis in both precision and accuracy for major and most minor elements.

Samples were coated with Ir to a thickness of <1 nm. A sample of 99.995% pure Fe metal was re-polished and coated alongside each round of experiments for use as an analytical blank to assess C surface contamination. After coating, all experiments and the C-blank were cleaned with an Evactron 25/45 RF oxygen plasma cleaner immediately prior to SDD-EDS analyses to remove C surface contamination; however, some surface C survived through to the analyses. Metal analyses were made by collecting an SDD-EDS spectrum for 50 s at operating voltage of 15 kV and a beam current of 1 nA with a spot size of ∼12 × 12 μm. Standards were pure Fe-metal, pure Ni metal, and graphite. Two Fe metal samples, Si metal, and SiC were used as secondary standards. The amount of C surface contamination was determined via analyses on the blank and the average C content from these analyses was subtracted from the total C detected in analyses of experimental alloys, typically resulting in analytical totals close to 100 wt.%. Silicate analyses were made using quantitative mapping mode at 1 nA over an area of ∼ 100 × 100 μm with a counting time of 1 ms per pixel. Standards were pyrope, diopside, cossyrite, and Al-rich enstatite, and secondary standards were a basaltic glass and San Carlos olivine.

2.3. Multiple-collector inductively-coupled plasma mass spectrometry (MC-ICP-MS) analyses

The remaining portion of each run product was crushed in an agate mortar and pestle. Metal and silicate phases were hand-picked under a binocular microscope and were easily discernible. Silicate separates were further purified with a strong magnet to ensure no contamination from small metal inclusions. Phase dissolutions and anion exchange chromatography procedures followed those of Craddock and Dauphas (2011). Phase separates and geostandards were dissolved in a three-step process: (1) 1 ml of concentrated HF + 0.5 ml of concentrated HNO_3, (2) 0.75 ml of concentrated HCl + 0.25 ml of concentrated HNO_3, and (3) 1 ml concentrated HCl + 0.5 ml concentrated HNO_3. During each step, solutions were kept in closed Savillex beakers on a hot plate at ∼150 °C overnight and were then dried down before the addition of new acids. After step (3), the samples were dissolved in 0.5–5

Table 1
Chemical compositions of experimental run products.

Expt. #	Phase	T (°C)	P (GPa)	Duration (h)	Starting metal	SiO_2	Al_2O_3	FeO	MgO	CaO	Fe	Si	C_{corr}	Total
PC 1350	Silicate	1850	1	0.5	None	47.56	3.83	5.69	37.07	5.20				99.35
	S. D.					0.55	0.14	0.06	0.62	0.21				
PC 1514	Silicate	1850	1	0.5		51.75	3.59	0.47	35.79	5.33				96.95
	S. D.					0.26	0.01	0.26	0.19	0.02				0.62
	Metal				$Fe_{91}Si_9$						90.3	4.95	4.43	99.70
	S. D.										0.48	0.11	0.54	0.77
PC 1529	Silicate	1850	1	0.5		51.0	3.78	0.60	35.3	5.47				96.89
	S. D.					0.38	0.15	0.05	0.47	0.14				0.65
	Metal				$Fe_{91}Si_9$						90.0	1.40	6.00	97.41
	S. D.										1.23	0.27	1.06	0.72
PC 1567	Silicate	1850	1	2		52.4	3.79	0.75	38.2	5.50				100.65
	S. D.					0.23	0.03	0.03	0.14	0.03				0.39
	Metal				$Fe_{95.5}Si_{4.5}$						93.2	0.87	5.02	99.10
	S. D.										0.58	0.04	0.67	0.97
PC 1570	Silicate	1850	1	0.5		52.3	3.86	0.79	38.1	5.59				100.68
	S. D.					0.29	0.05	0.22	0.11	0.04				0.41
	Metal				$Fe_{95.5}Si_{4.5}$						93.1	0.82	5.85	99.74
	S. D.										0.78	0.05	0.53	0.65
PC 1585	Silicate	1850	1	1		52.7	3.90	0.90	37.9	5.54				100.88
	S. D.					0.43	0.09	0.12	0.28	0.04				0.68
	Metal				$Fe_{95.5}Si_{4.5}$						92.5	0.90	5.97	99.40
	S. D.										0.59	0.10	1.04	1.13

Starting silicate composition (PC 1350) is from Elardo and Shahar (2017).
Values are in wt.%.
C_{corr} = carbon in alloy after correction for C surface contamination.

ml of 6M HCl, depending on Fe concentration, for column chemistry. Iron was purified using 1 ml of BioRad AG-1X8 200–400 mesh pre-cleaned resin loaded in BioRad Poly-Prep columns. Between 0.1 and 0.5 ml of sample in 6M HCl was added to the columns and after elution of matrix elements, the sample was collected in 0.4M HCl. Purified Fe was then dried down, redissolved in 6M HCl, and the column chemistry was repeated with new resin. Afterward, purified Fe was dissolved in 5 ml of 0.3M HNO_3 for isotopic analysis.

Isotopic analyses were conducted in pseudo-high-resolution mode on the Nu Instruments Plasma II MC-ICP-MS at GL, which has a fixed array of 16 Faraday collectors each with a 10^{11} Ω amplifier. Samples and the standard (IRMM-524a) were analyzed at a concentration of ~2.5–4 ppm ^{56}Fe in 0.3M HNO_3 solutions. Instrumental mass fractionation was corrected for using sample-standard bracketing and interferences on $^{54}Fe^+$, $^{56}Fe^+$, and $^{57}Fe^+$ from ArN^+, ArO^+, and $ArOH^+$, respectively, were fully resolved using a 30 µm source slit and variable slits before the electrostatic analyzer filter. Mass resolution of ~10,000 was estimated using ^{56}Fe. ^{53}Cr was measured simultaneously and the ^{54}Fe voltage was corrected for the ^{54}Cr interference. Samples were analyzed 10–20 times with each analysis consisting of 20 cycles of ~4 s integrations. Metal and silicate samples were always measured back to back on the same day.

3. Results

Experiments resulted in assemblages consisting of FeO-poor peridotite melt in equilibrium with molten Fe–Si–C-alloys (Fig. 1, Table 1). As expected, the Si-bearing starting metal compositions resulted in some reduction of FeO in the silicate melt and the oxidation of Si^0. The FeO contents of peridotite melts in our experiments ranged from 0.47 to 0.90 wt.%. The Fe-alloys contained between 0.82 and 4.95 wt.% Si (1.34–8.14 atom % Si). Similar chemical compositions of metal and silicate melts across similar experiments of different durations (Table 1) indicated that 30 min was sufficient to reach chemical equilibrium.

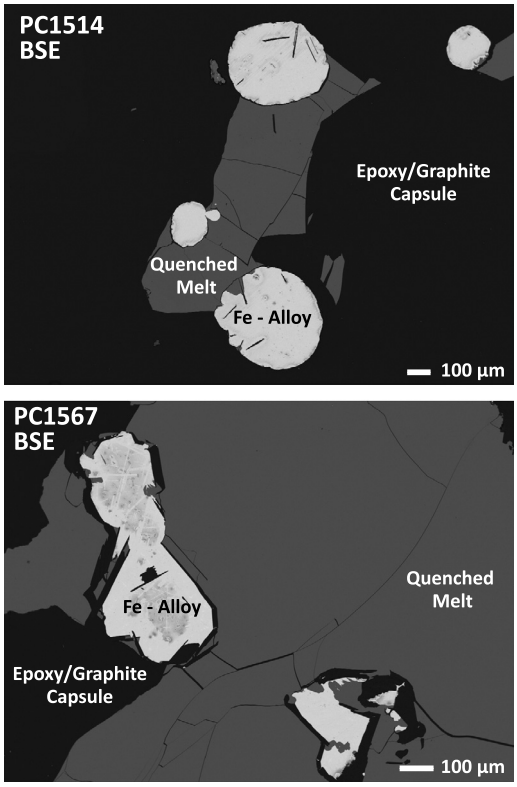

Fig. 1. Backscattered electron (BSE) images of two experiments from this study. Black regions are epoxy or graphite from the sample capsule. Gray regions are quenched melt and the bright regions are Fe–Si–C-alloy. The patchy discoloration on the surface of some of the alloys is oxidation from polishing and black inclusions in the alloys are graphite from the sample capsule.

Isotopic equilibrium was tested with the three-isotope exchange method (Shahar et al., 2008, 2017) and a time series. For each experiment reported here, both silicate and metal frac-

Table 2
Iron isotopic compositions of geostandards and experimental run products.

Sample	Phase	*n*	δ^{56}Fe (‰)	2SE	δ^{57}Fe (‰)	2SE	Δ^{56}Fe (‰)	2SE	$\Delta^{57}Fe_{Metal\text{-}Silicate}$ (‰)	2SE
Geostandards										
AGV-2		14	0.077	0.016	0.129	0.037	−0.010	0.027		
Accepted values[a]			*0.105*	*0.011*	*0.146*	*0.016*				
BIR-1		16	0.052	0.042	0.054	0.074	0.016	0.027		
Accepted values[a]			*0.053*	*0.015*	*0.087*	*0.023*				
BHVO-2		14	0.088	0.018	0.191	0.026	−0.042	0.026		
Accepted values[a]			*0.114*	*0.011*	*0.174*	*0.016*				
Experiments										
PC 1514	Silicate	13	−1.545	0.049	−1.344	0.062	−0.634	0.018	0.072	0.085
	Metal	10	−1.512	0.032	−1.272	0.059	−0.650	0.035		
PC1529[b]	Silicate	11	−2.770	0.029	−2.552	0.048	−1.040	0.030	−0.013	0.054
	Metal	11	−2.765	0.022	−2.565	0.025	−1.026	0.019		
PC1567	Silicate	10	−1.425	0.027	−1.178	0.038	−0.626	0.017	−0.012	0.063
	Metal	10	−1.422	0.025	−1.190	0.050	−0.616	0.036		
PC1570	Silicate	10	−1.400	0.027	−1.230	0.051	−0.566	0.027	0.059	0.061
	Metal	11	−1.366	0.025	−1.171	0.034	−0.572	0.022		
PC 1585	Silicate	19	−1.399	0.014	−1.170	0.028	−0.605	0.026	0.059	0.047
	Metal	20	−1.335	0.017	−1.111	0.038	−0.582	0.026		

[a] Values from Craddock and Dauphas (2011).
[b] A lower metal/silicate in this experiment resulted in more negative δ^{57}Fe values than other experiments.

tions had the identical Δ^{56}Fe values (i.e., departures from mass-dependency) within analytical error, indicating they lie on the same secondary mass fractionation line (Table 2). Additionally, three experiments ranging in duration from 0.5 to 2 h resulted in identical $\Delta^{57}Fe_{Metal\text{-}Silicate}$ within analytical error. Therefore, we conclude that the experiments reported here closely approached isotopic equilibrium. Two recent studies have argued that complex kinetic pathways to equilibrium in three isotope exchange experiments would create difficulties in determining the correct equilibrium fractionation factor between two phases (Cao and Bao, 2017; Bourdon et al., 2018); however, such concerns are only relevant for studies in which an extrapolation to a secondary fractionation line using a series of unequilibrated experiments is used and are thus not relevant for our group's work. The Fe isotopic fractionation between metal and silicate (i.e., $\Delta^{57}Fe_{Metal\text{-}Silicate} = \delta^{57}Fe_{Metal} - \delta^{57}Fe_{Silicate}$) for these experiments range between -0.013 ± 0.05‰ (2SE) and 0.072 ± 0.085‰ (Fig. 2, Table 2). Analyses of the AGV-2, BIR-1, and BHVO-2 geostandards were similar to accepted values.

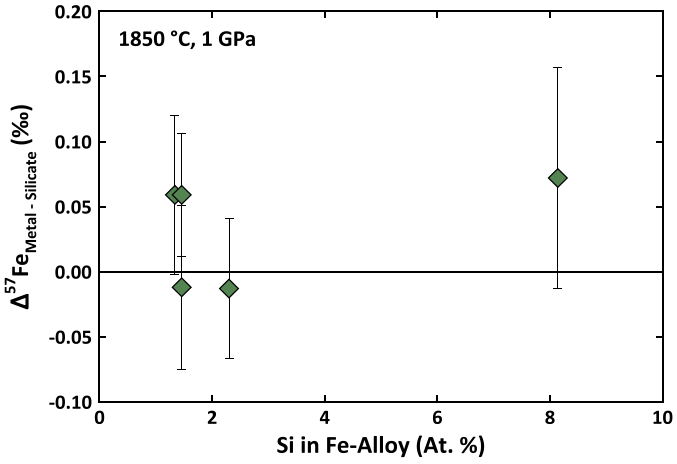

Fig. 2. Metal–silicate fractionation factors at 1850 °C and 1 GPa for Fe isotope exchange experiments vs. the amount of Si in at. % in the Fe-alloy. Uncertainties are 2 standard errors.

4. Discussion

4.1. Does Si in planetary cores have an effect on Fe isotope fractionation at low pressure?

The results of our experiments containing Fe–Si–C-alloys are consistent with previous results from our group for experiments with S- and Fe–Ni-alloys (Fig. 3), but with the exception of one experiment, do not show resolvable effects on their own. The $\Delta^{57}Fe_{Metal\text{-}Silicate}$ at 1850 °C of the experiment containing the most Si-rich metal is the highest among our Si-bearing experiments. The fractionation is 0.072 ± 0.085‰ and falls on the trend in the Ni- and S-bearing experiments (Fig. 3), although this experiment is not resolved from 0‰. These results do not definitely demonstrate an effect attributable to Si. However, their consistency with previous experiments combined with the observations Fe isotope fractionation between silicates and Fe–Si metal in aubrite meteorites (Jordan et al., 2019) suggests that experiments with higher Si in Fe alloys may follow the behavior suggested by Elardo and Shahar (2017) wherein elements that substitute for Fe in the alloy structure drive Fe isotope fractionation. As only one of the Si-bearing experiments had a $\Delta^{57}Fe_{Metal\text{-}Silicate}$ at 1850 °C greater than 0‰ outside of uncertainty, it is difficult to draw any definitive conclusions from this dataset alone. Experiments with greater amounts of Si in the alloy were attempted but are not reported due to the large analytical uncertainties on the isotopic compositions of the silicate fractions. The recovery of sufficient metal-free silicate to enable robust analyses was extremely challenging due to the low FeO abundances in the melt. In sections below, we will consider the new Si-bearing experiments alongside previous experiments from our group and others in an attempt to elucidate the causes of Fe isotopic fractionation behavior and its consequences for the smaller terrestrial planets and asteroids.

4.2. Iron isotope fractionation during core formation: a metallic structural effect?

The structures of metallic liquids offer insights into the Fe isotopic fractionation behavior observed in experiments. Core-relevant metallic liquids with and without light elements (i.e., S, Si, C) have been studied *in situ* using synchrotron X-ray diffraction (e.g., Sanloup et al., 2000, 2002, 2004; Kono et al., 2015; Shibazaki et al., 2015). Radial distribution functions derived from

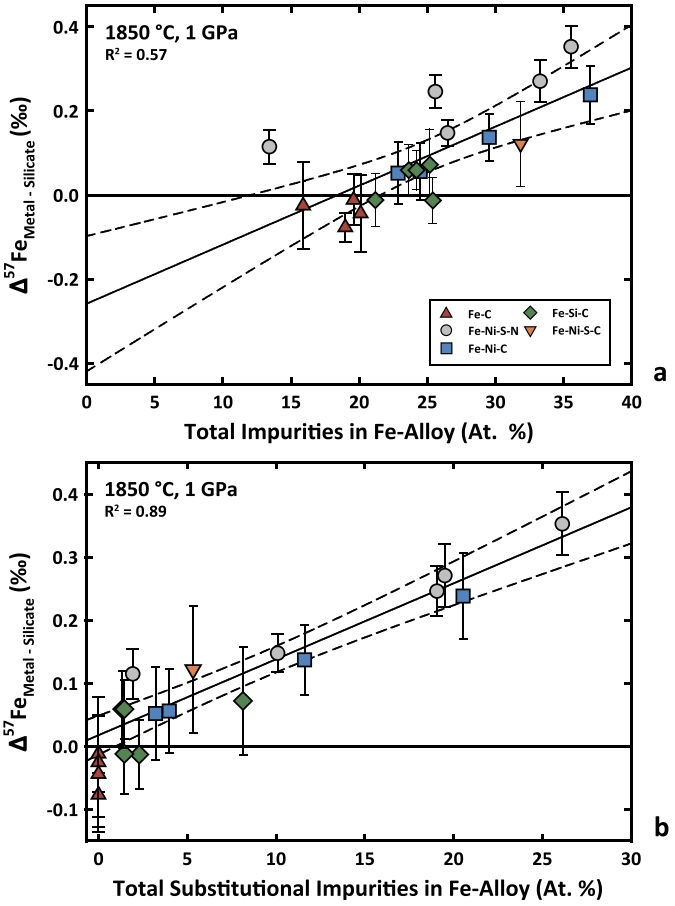

Fig. 3. Metal–silicate fractionation factors at 1850 °C and 1 GPa for Fe isotope exchange experiments as a function of the total amount of non-Fe elements in the Fe-alloy (a) and the total amount of non-Fe elements that substitute for Fe atoms in the Fe-alloy structure (i.e., Ni, S, Si) (b). Solid and dashed lines are least-squares linear regressions and 95% confidence envelopes, respectively. The Fe–C data are not included in the regression in (b) (see section 4.3). The Fe–Si–C data are from this work. The Fe–Ni–S–N experiments are from Shahar et al. (2015) corrected to 1850 °C using the $1/T^2$ relationship. The Fe–C and Fe–Ni–C experiments are from Elardo and Shahar (2017). The single Fe–Ni–C–S experiment is PC-564b from Poitrasson et al. (2009) corrected to 1850 °C. Uncertainties are 2 standard errors.

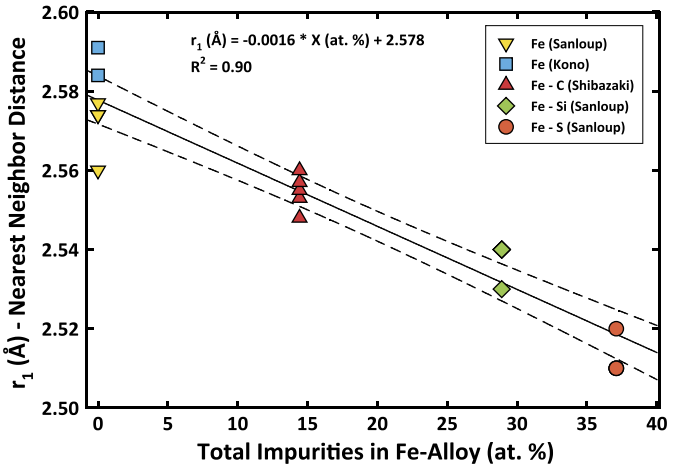

Fig. 4. A plot of nearest neighbor distances in Å for Fe atoms in molten Fe and Fe-alloys as a function of the total amount of non-Fe elements in each alloy. Solid and dashed lines are a least-squares linear regression and 95% confidence envelope, respectively. Data for molten Fe are from Sanloup et al. (2000) and Kono et al. (2015). Data for molten Fe–C-alloys is from Shibazaki et al. (2015). Data for molten Fe–Si and Fe–S-alloys are from Sanloup et al. (2002). For comparison, pure molten Ni has an r_1 of ~2.49–2.48 Å (Schenk et al., 2002).

these measurements have shown that Fe-rich metallic liquids retain short- to medium-range order and allow for the determination of nearest neighbor atomic distances (r_1). This is potentially insightful for isotopic studies, as bond stiffness affects a phase's preference for light vs. heavy isotopes of an element, with shorter, stiffer bonds generally favoring heavy isotopes (e.g., Young et al., 2015).

Between ambient pressure and ~5 GPa, and ~1200 to 2000 °C, r_1 is not strongly dependent on either pressure or temperature, but it does exhibit a correlation with composition. Nearest neighbor distances in molten alloys decrease linearly from ~2.58 to ~2.51 Å with increasing abundances of alloying elements from 0 to ~40 at.% (Fig. 4). Similar to $\Delta^{57}Fe_{Metal\text{-}Silicate}$ values (Fig. 3), the r_1 distances of molten Fe-rich alloys appear to be dependent on the total abundance of impurity elements in the molten Fe-alloy, independent of the identity of the elements within the resolution of the measurements. Therefore, we suggest that shortening of Fe bonds in molten Fe-alloys due to the addition of alloying elements may be the primary mechanism for our observed Fe isotope fractionation behavior. This effect would be directly relevant to core-mantle equilibration in the Moon, Mercury, differentiated asteroids such as Vesta, and low-pressure core formation on Mars. There appears to be a structural transition in molten Fe-alloys at ~5 GPa, near the bcc-fcc-liquid triple point (Sanloup et al., 2000; Kono et al., 2015; Shibazaki et al., 2015). It is unclear what effect this structural transition will have on Fe isotope fractionation; however, we note that the transition results in further shortening of r_1, so it is possible that pressures >5 GPa could enhance Fe isotope fractionation. This model is not without some assumptions and complexities that require experimental verification. We assume that Ni has the same effect on r_1 as S, C, and Si. To our knowledge, there are no similar studies on the effect of Ni on r_1 in Fe-rich alloys. However, the r_1 distance in pure molten Ni (~2.48–2.49 Å; Schenk et al., 2002) is shorter than that in pure Fe, so this assumption may be valid.

4.3. Substitutional vs. interstitial element partitioning

Elardo and Shahar (2017) proposed that elements which substitute for Fe in the alloy structure, such as Ni, S, and Si, have a greater effect on the bonding environment of Fe atoms and the magnitude of Fe isotope fractionation than elements such as C and N, which partition into interstitial sites in the Fe-alloy. This model is supported by a few lines of evidence. The expectation from first principles is that metals should favor heavy Fe isotopes relative to silicates. Metallic bonds have delocalized, itinerant electrons which form shorter and stiffer bonds than localized electrons, and thus metallic bonds should favor heavy Fe isotopes over Fe–O bonds in silicates (Young et al., 2015). However, if we regress the metallic compositional effect on $\Delta^{57}Fe_{Metal\text{-}Silicate}$ in terms of the total amount of impurities in the metal, we would predict that the δ^{57}Fe of pure Fe should be significantly lighter than silicate melt by >0.2‰ at 1850 °C (Fig. 3a). This regression would also predict a sign change in $\Delta^{57}Fe_{Metal\text{-}Silicate}$ at ~18 at.% total impurities, which has no foundation in theory. Alternatively, if we regress the metallic compositional effect in terms of the total amount of only substitutional impurities (Fig. 3b), we predict no sign change and that all Fe-alloys should be heavier than silicate melt, in line with the expectations from first principles. At 1850 °C, the compositional effect of substitutional impurities can be expressed by following relationship:

$$\Delta^{57}Fe_{Metal\text{-}Silicate} = 0.0120 * X_{Sub} + 0.0176, \qquad R^2 = 0.89 \quad (1)$$

where X_{Sub} is the total at.% of substitutional elements (i.e., Ni, S, and Si) in the metal phase. This regression includes all experiments in Fig. 3 with the exception of the Fe–C set, which contain no substitutional impurities in the Fe-alloys. We can also parameterize $\Delta^{57}Fe_{Metal\text{-}Silicate}$ to include the effect of temperature, as equilibrium stable isotope fractionation scales as $1/T^2$:

$$\Delta^{57}Fe_{Metal\text{-}Silicate} = \frac{5.41 * 10^4 * X_{Sub} + 7.93 * 10^4}{T^2} \quad (2)$$

where T is temperature in K. Interestingly, the effects of individual element impurities on $\Delta^{57}Fe_{Metal\text{-}Silicate}$ are more tightly correlated in the substitutional-only regression than in the all-impurity regression (Fig. 3b). This is consistent with the data presented in Fig. 4, which shows that all impurities in Fe-alloys have essentially the same effect on nearest neighbor distance in the alloy. Therefore, we conclude that Equation (2) most accurately describes the effects of composition and temperature on the magnitude of Fe isotope fractionation between molten Fe-rich metal and molten peridotite based on currently available data. This is also consistent with the compositions of magmatic iron meteorites, which are nearly ubiquitously heavy (Poitrasson et al., 2005; Williams et al., 2006), with metal–silicate fractionation observed in aubrite meteorites that contain Fe–Si-alloys (Jordan et al., 2019), and with the fractionation observed in pallasite meteorites (Poitrasson et al., 2005).

A complexity in this model is that the presence of C in Fe-alloys also appears to shorten nearest neighbor distances with a similar effect to S and Si (Fig. 4), yet apparently does not have a corresponding effect on Fe isotope fractionation. The reason for this behavior is unknown and more work is needed to further investigate the effects of interstitial elements.

4.4. Reconciling differing experimental results from the literature

Groups investigating equilibrium Fe isotope fractionation during core formation have come to disparate conclusions using similar techniques. Using piston-cylinder and multi-anvil experiments, Poitrasson et al. (2009) and Hin et al. (2012) argued that metal-silicate equilibration does not result in a resolvable fractionation of Fe isotopes. Conversely, Shahar et al. (2015) and Elardo and Shahar (2017) found resolvable, relatively large fractionations that correlated with the composition of the metal phase. Here we attempt to reconcile these observations.

Poitrasson et al. (2009) presented the results of seven experiments designed to investigate Fe isotope fractionation. Their starting materials consisted of a devolatilized chondrite composition with one exception in which S was not present in the system. Six of the seven experiments were conducted at 2000 °C and ranged in pressure from 2–7.7 GPa, with durations between <2 min and 10 min. The average $\Delta^{57}Fe_{Metal\text{-}Silicate}$ of those six experiments was 0.047 ± 0.063‰, despite the fact that the Fe-alloys contained Ni and S.

The seventh experiment from Poitrasson et al. (2009) is informative in resolving this discrepancy. That experiment (PC-564b) was conducted at 1750 °C, 1 GPa, and most importantly, at 30 min it was their longest duration experiment. The bulk metal phase consisted of a C-rich Fe–Ni–S melt. An immiscible S-rich Fe–Ni–C melt was also present; however, the C-rich melt was far more abundant so it likely controlled the measured metal composition. Although Poitrasson et al. (2009) did not discuss the results of this experiment in detail, it yielded a $\Delta^{57}Fe_{Metal\text{-}Silicate}$ of 0.134 ± 0.101‰ and is their only fractionation factor resolved from 0‰. This value agrees well with our group's results (Fig. 3). Shahar et al. (2015) showed that an experiment conducted for 5 min at 1650 °C and 1 GPa did not come to isotopic equilibrium, as revealed by the three-isotope exchange method. Furthermore, Shahar et al. (2008) demonstrated that chemical equilibrium is reached faster than isotopic equilibrium in isotope exchange experiments, making a sufficiently long time series of the utmost importance. The shortest experiment in the time series from Elardo and Shahar (2017), lasting 30 min at 1850 °C, did achieve equilibrium and had the same $\Delta^{57}Fe_{Metal\text{-}Silicate}$ as longer runs up to 3 h. The experimental temperatures cannot fully explain the differences in the Poitrasson et al. (2009) results. Adjustment of the $\Delta^{57}Fe_{Metal\text{-}Silicate}$ of 0.134 ‰ at 1750 °C to 2000 °C using a $1/T^2$ relationship results in a $\Delta^{57}Fe_{Metal\text{-}Silicate}$ of 0.11‰, which is higher than the average of their 2000 °C experiments by more than a factor of two. We conclude that it is likely PC-564b is the only experiment from Poitrasson et al. (2009) that achieved isotopic equilibrium and therefore we have included it in our compositional regression (Fig. 3 and Eqs. (1) and (2)).

Hin et al. (2012) presented the results of ten experiments designed to investigate fractionation at lower temperature. In order to lower the melting point of their Fe-alloys to below their run conditions of 1250–1300 °C and ~1 GPa, they added ~25 wt.% Sn to their metal starting materials. Capsules were either graphite, which introduced C into the Fe–Sn-alloys, or SiO_2 glass. Durations were between 0.4 and 16 h and equilibrium was assessed with a time series. The largest deviation from 0‰ in $\Delta^{56}Fe_{Metal\text{-}Silicate}$ outside of uncertainty observed by Hin et al. (2012) was 0.02‰ in a single experiment at 1250 °C and therefore they argued that core formation would not result in a detectable fractionation of Fe isotopes.

The experiments of Hin et al. (2012) are difficult to interpret for a few reasons. Firstly, the phase relations in the Fe–Sn–C system are poorly known. If we consider the C-free ambient pressure Fe–Sn binary phase diagram (Hansen, 1958), the alloys in their experiments at 1250–1300 °C should have been below the liquidus. The added pressure of the experiments should increase the liquidus temperature, so it is likely that the Hin et al. (2012) experiments contained two Fe–Sn phases. Backscattered electron images clearly showed two metallic phases in at least one experiment, although the composition of only one phase is reported. This feature was interpreted to be the result of exsolution upon quench; however, the morphology of the coexisting alloys in their images (fully separated, discrete phases with smooth boundaries; Fig. 1c in Hin et al., 2012) indicate it is more likely to be an equilibrium feature. Together, these observations make it difficult to interpret the compositional relationships of the metallic phases relative to the isotopic compositions. Secondly, the effects of Sn in Fe-alloys on the fractionation of Fe isotopes are difficult to determine. The metallic radii difference between Sn and Fe leaves the former on the very upper edge of the substitutional alloy "favorable zone" defined by Hume-Rothery (1966), which is the range in metallic radii that are favorable to the formation of a substitutional alloy with Fe. However, Sn does not appear to have the same effect on Fe isotopic fractionation that has been demonstrated by our experiments for other substitutional elements (Fig. 3b). One possibility is that Sn affects the structure of the Fe–Sn-alloys in a way that differs from Ni, S, and Si. The Fe–Sn phase diagram shows a complex liquidus topology, including a region of two-liquid immiscibility, indicative of non-ideal mixing between Fe and Sn. Because the effects of Sn on the bonding environment of metals are poorly known, we strongly advise against the use of Sn in future experimental studies of isotope fractionation.

Another possibility for the results in Hin et al. (2012) is incomplete separation of the metal and silicate phases. It is useful to remember that measured fractionation factors in isotope exchange experiments are minimum values, as impure phase separates will artificially produce fractionation factors closer to 0‰ than the true value. Whatever the cause, the results of Hin et al. (2012) are in-

consistent with multiple other piston cylinder studies (Shahar et al., 2015; Elardo and Shahar, 2017) and thus we have not included their data in our regressions.

4.5. Estimates of the iron isotope compositions of planetary mantles using experiments

Appropriate values of $\Delta^{57}Fe_{Metal\text{-}Silicate}$ to model core formation were calculated using Eq. (2). Estimated ranges of core-mantle equilibration temperatures were 2050–3350 K for the Moon, 1900–2300 K for Mars, and 1725–2000 K for Vesta (Righter and Drake, 1996; Righter and Chabot, 2011; Pringle et al., 2013; Steenstra et al., 2016a, 2016b). Estimated ranges for X_{sub} in at.% in planetary cores were 7.9–61.7 for the Moon, 8.0–36.4 for Mars, and 7.5–28.4 for Vesta (Dreibus and Wänke, 1980; O'Neill, 1991; Righter and Drake, 1996; Mittlefehldt et al., 1998; Weber et al., 2011). We can then calculate a range of $\delta^{57}Fe_{Mantle}$ for each planetary mantle with the isotope mass balance relationship:

$$\delta^{57}Fe_{Bulk\ Planet} = \left(\Delta^{57}Fe_{Metal\text{-}Silicate} + \delta^{57}Fe_{Mantle}\right) \times (1 - fFe_{Mantle}) + \delta^{57}Fe_{Mantle} \times fFe_{Mantle} \quad (3)$$

where fFe_{Mantle} is the mass fraction of Fe in the bulk silicate portion of each planetary body. Ranges for fFe_{Mantle} were calculated using estimates for the core mass fraction and bulk silicate Fe content of 0.024 and 5.51 wt.%, respectively for the Moon, 0.206 and 13.4 wt.% for Mars, and 0.180 and 11.15 wt.% for Vesta (Dreibus and Wänke, 1985; Lodders and Fegley, 1997; Ruzicka et al., 1997; Longhi, 2006; Russell et al., 2012; Steenstra et al., 2016b). We assume that $\delta^{57}Fe_{Bulk\ Planet}$ is equal to the chondritic value of ~0‰. Our calculations update those presented by Elardo and Shahar (2017) by incorporating our new experiments in Eqs. (1) and (2). We do not estimate Earth's mantle because it is unlikely our experiments at 1 GPa capture the appropriate bonding environments for Fe at terrestrial core formation conditions. The $\delta^{57}Fe$ of the BSE (or at least the sampled upper mantle) is best constrained by the compositions of peridotite xenoliths (Dauphas et al., 2017), which have a strong peak in compositions $\delta^{57}Fe = -0.039$‰, although some mantle heterogeneity and uncertainty regarding the BSE value certainly exists (Poitrasson et al., 2013; Williams and Bizimis, 2014). Our model predicts that the $\delta^{57}Fe_{Mantle}$ is between −0.01‰ to −0.12‰ for the Moon, −0.06‰ to −0.33‰ for Mars, and −0.08‰ to −0.33‰ for Vesta. The model predicts a more restricted range for the lunar mantle due to the small size of the lunar core (i.e., a high fFe_{Mantle}) and the ranges are a function of the ranges in estimates of core-mantle equilibration temperature and X_{sub} listed above.

4.6. Estimates of the iron isotope compositions of planetary mantles using samples

4.6.1. The Moon

Lunar basalts span a large range in $\delta^{57}Fe$ from roughly chondritic compositions in some picritic volcanic glasses to very heavy values in high-Ti basalts (Poitrasson et al., 2004; Weyer et al., 2004), leading some workers to conclude that the heavy average composition of lunar basalts is indicative of a heavy bulk silicate Moon. Although the low-Ti mare basalt suite has been previously used to estimate the $\delta^{57}Fe$ of bulk Moon (Poitrasson et al., 2004; Dauphas et al., 2017), these samples are partial melts of lunar mantle source regions that formed after significant amounts (>80%) of crystal fractionation in the magma ocean as evidenced by ubiquitous negative Eu anomalies. Even small (e.g., <0.1‰) mineral-melt fractionation factors could cause significant Fe isotope fractionation over the course of magma ocean fractional crystallization (e.g., Wang et al., 2015). Thus, it is unlikely that the $\delta^{57}Fe$ of low-Ti basalt source regions is similar to that of the bulk silicate Moon. Additionally, samples of the Mg-suite plutonic rocks have been used to estimate the composition of the lunar mantle because they have an Mg# close to that of the bulk Moon (Wang et al., 2015; Sossi and Moynier, 2017). However, the Mg-suite are cumulate rocks, not magmatic liquid compositions, and their parental melts incorporated significant amounts of both crustal anorthosite and the highly geochemically fractionated KREEP reservoir (Papike et al., 1996; Elardo et al., 2011; Shearer et al., 2015), so their positive $\delta^{57}Fe$ ranging from 0.05–0.10‰ (Sossi and Moynier, 2017) is reflective of Fe sourced from multiple geochemical reservoirs, some of which have been highly fractionated, and thus will not be reflective of the $\delta^{57}Fe$ of the bulk silicate Moon.

In order to estimate the $\delta^{57}Fe$ of a primitive lunar mantle source region, Elardo and Shahar (2017) used the $\delta^{57}Fe$ of -0.027 ± 0.050‰ of the Apollo 15 green glass from Poitrasson et al. (2004). The Apollo 15 green glasses represent the most primitive mantle melts from the Moon currently known (Longhi, 1992), so they are the lunar samples most likely to record a mantle $\delta^{57}Fe$ close to the bulk silicate Moon value (also see Supplementary Information in Elardo and Shahar, 2017). Measured compositions of the green glass are somewhat varied (Weyer et al., 2004; Sossi and Moynier, 2017). This could be the result of variability in the five different magma compositions present in the green glass deposit or possibly the accumulation of isotopically light Fe deposited on glass bead surfaces during fire fountaining. The latter has been suggested to have affected the isotopic compositions of more volatile elements such as Zn (Kato et al., 2015); however, given that Fe is significantly less volatile than Zn, that the volcanic glass beads contain ~3 orders of magnitude more Fe than Zn, and that glass bead coatings are volumetrically very small compared to the beads themselves, it remains to be demonstrated that Fe in bead coatings has an effect on the measured $\delta^{57}Fe$ of the glasses. Therefore, using the composition of the Apollo 15 green glass and the $\Delta^{57}Fe_{Mantle\text{-}Melt}$ of −0.07‰ estimated by Elardo and Shahar (2017) for melting of reduced mantles (see the Supplementary Information in that study for rationale for this fractionation factor), the $\delta^{57}Fe$ of the green glass source region would be -0.10 ± 0.05‰. We consider this value to be best sample-based estimate available for a primitive lunar mantle source region and is perhaps close to that of the bulk silicate Moon. This mantle value agrees well with the range predicted by our model (Fig. 5).

4.6.2. Mars

There is no obvious single basaltic shergottite that could be used to estimate the $\delta^{57}Fe$ of the primitive martian mantle. Sossi et al. (2016a) corrected the measured $\delta^{57}Fe$ of a suite of martian samples to account for accumulation of olivine and pyroxene (assuming a $\Delta^{57}Fe_{Mineral\text{-}Melt}$ of −0.10‰) to calculate parental melt compositions and subsequently the $\delta^{57}Fe$ at the Mg# estimated for the bulk martian mantle. Their estimate of the $\delta^{57}Fe$ of the martian mantle is -0.04 ± 0.03‰. Although Sossi et al. (2016a) provided the best estimates for the $\delta^{57}Fe$ values of magmas parental to the martian meteorites available, they did not take into account fractionation during mantle partial melting. Experimentally determined liquidus multiple saturation points for martian basalts indicate they are derived from mantle source regions consisting of olivine and low-Ca pyroxene (e.g., Musselwhite et al., 2006), so by definition that −0.10‰ fractionation must apply during mantle melting as well, as both fractionation during melting and subsequent fractional crystallization in the melt should have similar effects when the same phases are present. If we take the lightest (i.e., most primitive) $\delta^{57}Fe$ for a martian parental liq-

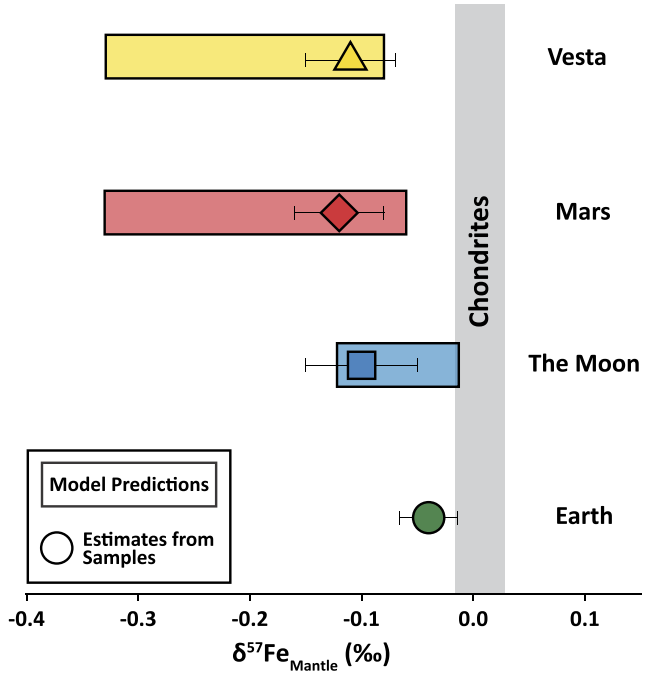

Fig. 5. A plot of estimates of the δ^{57}Fe of the bulk silicate portions of Earth, the Moon, Mars, and Vesta. Shaded bars represent the ranges derived from our experimental model of fractionation during core formation. Data points for the Moon, Mars, and Vesta are estimates of primitive mantle source regions derived from the δ^{57}Fe values basaltic samples (see section 4.6). Data point for Earth's mantle is the composition of the peak in the global peridotite dataset from Dauphas et al. (2017 and references therein). Gray bar is the 95% confidence interval for the average composition of all chondritic meteorites from Craddock and Dauphas (2011).

uid (LAR 06319) calculated by Sossi et al. (2016a) and apply a $\Delta^{57}Fe_{Mantle\text{-}Melt}$ of $-0.10‰$, we calculate a δ^{57}Fe of $-0.12 \pm 0.04‰$ for its mantle source region, within the range predicted by our model (Fig. 5). Clearly there is heterogeneity in the martian mantle, given the scatter in Mg# vs. δ^{57}Fe for martian parental liquids (Sossi et al., 2016a), which could be attributed to magma ocean crystallization, mantle mixing during convection, and/or previous episodes of melt extraction. However, we consider $-0.12‰$ to be a reasonable estimate for the δ^{57}Fe of a primitive martian mantle source region.

4.6.3. Vesta

The δ^{57}Fe values of non-cumulate eucrites likely have a different relationship to the δ^{57}Fe of the bulk vestian mantle than do basaltic samples from Earth, the Moon, and Mars. Eucrites have been proposed to represent partial melts of an undifferentiated, chondritic mantle (Stolper, 1977) or residual liquids from crystallization of a magma ocean (Righter and Drake, 1997; Ruzicka et al., 1997). However, each of these models have difficulty explaining the bulk compositions of eucrites, their limited compositional range, and/or their relationships to diogenites (Mandler and Elkins-Tanton, 2013). A variation of the magma ocean residual liquid model proposed by Mandler and Elkins-Tanton (2013) showed that 60–70% equilibrium crystallization of a vestian magma ocean followed by extraction of the residual liquid to shallow magma chambers that are periodically recharged can explain the narrow compositional range in the eucrites while simultaneously producing diogenite cumulates. This model may also account for why the eucrites exhibit a narrow range in δ^{57}Fe. Both equilibrium crystallization of the vestian magma ocean and replenishment of eucrite magma chambers would limit the range in δ^{57}Fe compared with that produced by fractional crystallization.

In all models of eucrite petrogenesis from a magma ocean, the non-cumulate eucrites with the lightest δ^{57}Fe would be the most primitive, as fractionation during crystallization of the residual melts would enrich the melt in heavy isotopes (Weyer and Ionov, 2007; Craddock et al., 2013; Teng et al., 2013; Dauphas et al., 2014). Therefore, we use the δ^{57}Fe of $-0.035 \pm 0.042‰$ the eucrite Juvinas (Poitrasson et al., 2004), the lightest δ^{57}Fe measured for a non-cumulate eucrite, and the $\Delta^{57}Fe_{Mantle\text{-}Melt}$ of $-0.07‰$ estimated by Elardo and Shahar (2017) to estimate the δ^{57}Fe of a primitive mantle source region in Vesta to be $-0.11 \pm 0.04‰$. This primitive mantle source region composition agrees well with the mantle range predicted by our core formation model (Fig. 5).

4.7. Are volatile depletion processes recorded by iron isotopes?

Fractionations of Fe isotopes relative to chondrites in various planetary sample suites have been attributed by some workers to volatile depletion processes. Poitrasson et al. (2004) suggested that the Moon-forming giant impact may have fractionated Fe isotopes, leaving the residual silicate Moon and Earth heavy. Sossi et al. (2016a) suggested that fractionation during volatile loss events was more widespread and occurred in either the nebular or post-nebular phase of accretion based on an apparent correlation between Fe/Mn and δ^{57}Fe in basalts from Earth, the Moon, Mars, and Vesta, and in ureilites and angrites. However, neither model accounted for Fe isotope fractionation during core formation. Additionally, the apparent correlation between Fe/Mn and δ^{57}Fe is predicated, in part, on a heavy isotopic composition for Earth, which is still heavily debated (see Dauphas et al., 2017), and also implies that Vesta is one of the least volatile depleted differentiated bodies despite geochemical evidence that it is one of the most depleted (e.g., Mittlefehldt, 1987), which suggest that the correlation may be an artifact arising from the assumed bulk δ^{57}Fe of each body.

In Fig. 6a we compare the Fe/Mn of Earth, the Moon, Mars, and Vesta (O'Neill and Palme, 2008) to peak δ^{57}Fe value of terrestrial peridotites and the calculated δ^{57}Fe of the mantle source regions of the Apollo 15 green glasses, basaltic shergottite LAR 06316, and the Juvinas eucrite. We do not consider the ureilites or angrites here because these meteorites groups have very complex mineralogy, geochemistry, and petrogenetic histories (e.g., Mittlefehldt et al., 1998) that do not make their δ^{57}Fe easily relatable to the bulk δ^{57}Fe of their parent bodies. Fig. 6a shows that there is no correlation between the δ^{57}Fe of primitive mantle source regions and Fe/Mn that would be indicative of Fe isotope fractionation by volatile depletion. The δ^{57}Fe and Fe/Mn of planetary mantles can be explained by a combination of isotope fractionation during core formation and elemental volatile depletion processes that do not affect Fe isotopes (Fig. 6a). Some Fe isotope fractionation via volatile depletion cannot be completely ruled out, as these processes are not mutually exclusive, and in a δ^{57}Fe vs. Fe/Mn plot these processes would qualitatively drive planetary mantles in different directions, making the deconvolution of their relative effects difficult.

Therefore, to further assess the possibility of Fe isotope fractionation during volatile depletion, we consider three elemental ratios that are diagnostic of volatile depletion (Halliday and Porcelli, 2001; O'Neill and Palme, 2008) but are not affected by core formation: Mn/Na, Rb/Sr, and K/U. Fig. 6b–d shows that there are no discernible correlations between the δ^{57}Fe of planetary mantles and these ratios. In all cases, the δ^{57}Fe of planetary mantles can be explained by a combination of the core formation process fractionating Fe isotopes and volatile depletion processes affecting the elemental Mn/Na, Rb/Sr, and K/U without noticeably fractionating Fe isotopes.

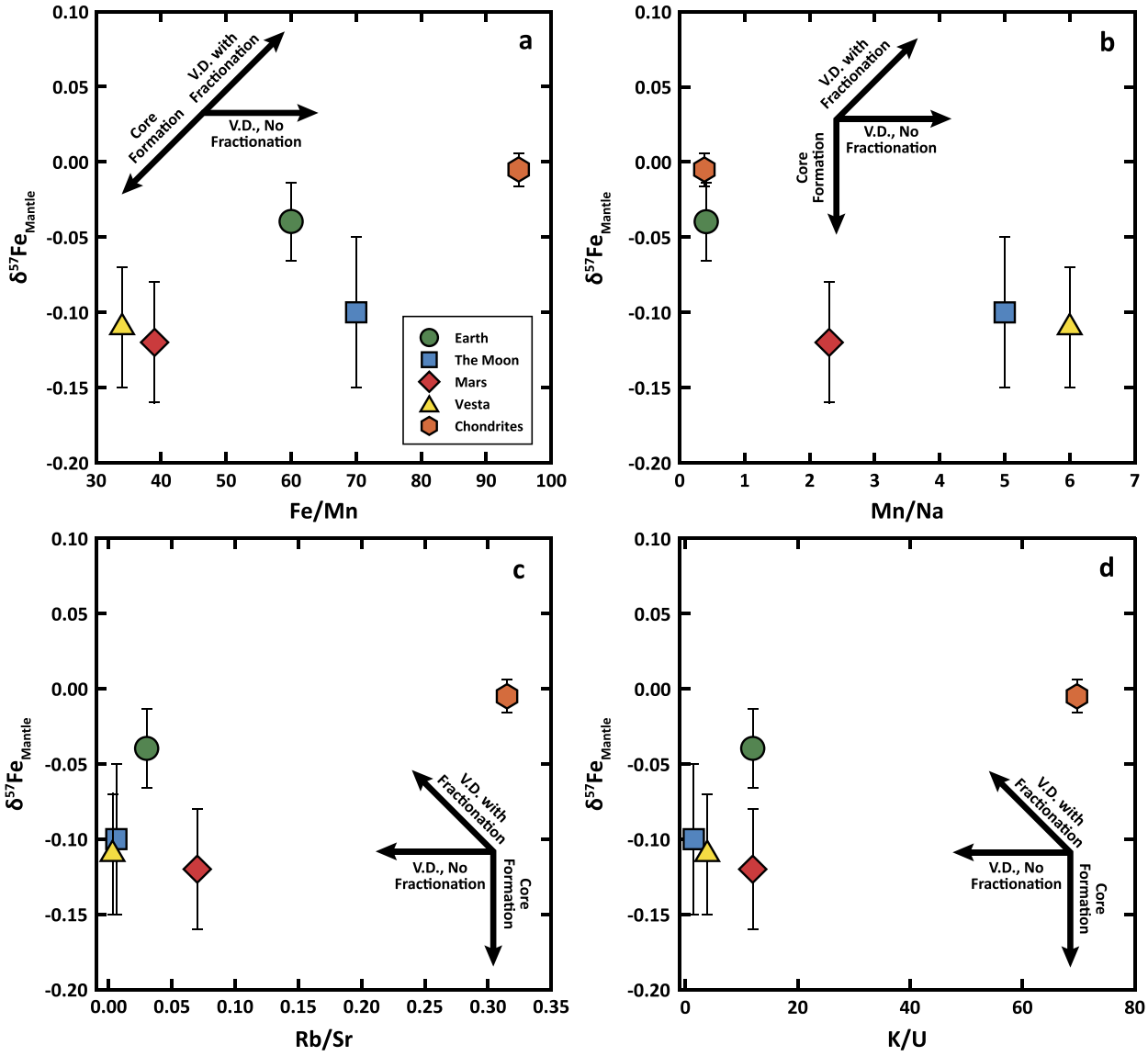

Fig. 6. Plots of the δ^{57}Fe of primitive mantle sources regions for the Moon, Mars, and Vesta calculated from basalt data (see section 4.6) and the peak in the global peridotite dataset from Dauphas et al. (2017 and references therein) vs. bulk silicate ratios for various indices of volatile depletion, Fe/Mn (a), Mn/Na (b), Rb/Sr (c), and K/U (d). The volatile element ratio data for the chondrite data points are for CI chondrites, whereas the δ^{57}Fe is the average for all chondrite groups. Ratios are from O'Neill and Palme (2008) and Halliday and Porcelli (2001). Arrows schematically indicate the directions that the processes of core formation, volatile depletion (V. D.) with Fe isotope fractionation, and volatile depletion without Fe isotope fractionation would move planetary mantles relative to chondrites.

4.8. Fe isotope evolution during planetary differentiation

Our schematic model for how Fe isotopes fractionate during accretion, differentiation, and mantle melting is shown in Fig. 7. The solar nebula was likely homogeneous in terms of Fe isotopes, as indicated by chondrites (e.g., Craddock and Dauphas, 2011). We do not find robust evidence of fractionation via volatilization during planetary accretion (e.g., Fig. 6), though its effects may have been overprinted by other processes. Experiments show that fractionation during core formation results in light mantles and heavy cores in the smaller planets and asteroids (Fig. 3). The higher temperatures during Earth's core formation and the effects of pressure on the bonding environment of Fe appear to have resulted in little to no fractionation in Earth's mantle, as evidenced by the global peridotite suite (e.g., Craddock et al., 2013; Dauphas et al., 2017). The Fe isotope difference between abyssal peridotites and MORBs, and the very wide range in δ^{57}Fe in lunar basalts demonstrate that mineral-melt equilibrium enriches the melt in heavy isotopes. Fractional crystallization of the lunar magma ocean likely created a heterogeneous mantle and further fractionation during subsequent mantle partial melting produced the range observed in lunar basalts. The more restricted range in shergottites and basaltic eucrites may be the result of non-representative sampling from those bodies, re-homogenization during mantle convection on Mars, and/or more restricted fractionation during equilibrium crystallization of the vestian magma ocean.

Acknowledgements

We are grateful to Mary F. Horan for her assistance in the Carnegie DTM chemistry lab. We thank Nancy Chabot and Franck Poitrasson for thorough and thoughtful reviews and Fred Moynier for his editorial handling. This work was funded by NSF grant EAR-1321858 to A. S. S. M. E. also acknowledges support from the Carnegie Institution for Science. This work was performed under the auspices of the U.S. Department of Energy by Lawrence Livermore National Laboratory under Contract DE-AC52-07NA27344. This is release number LLNL-JRNL-753799.

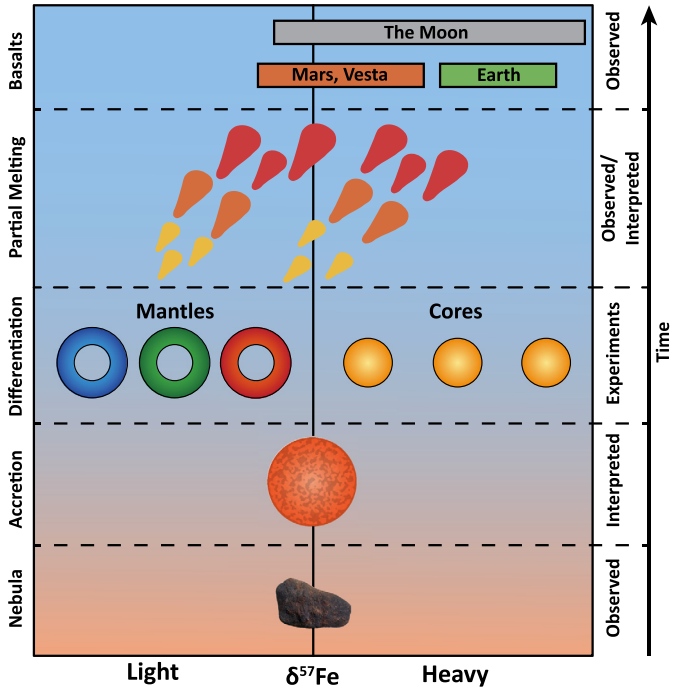

Fig. 7. A schematic model for the fractionation of Fe isotopes during planetary accretion, differentiation, and mantle melting (figure adapted from Sossi, 2017 based on the model presented by Elardo and Shahar, 2017). Planets and asteroids accrete from a nebula with the observed homogeneous Fe isotope composition of chondrites. Based on the lack of clear correlations between estimates of bulk planetary δ^{57}Fe and elemental indicators of volatile depletion processes (Fig. 6), we infer no fractionation during accretion. Core formation fractionates Fe isotopes, resulting in heavy cores and isotopically light mantles, at least at relatively low pressure. Mineral-melt fractionation during magma ocean crystallization will result in heterogeneous mantles, especially in regimes where fractional crystallization dominates (e.g., the Moon). Mineral-melt fractionation will also occur during mantle partial melting, as is observed in abyssal peridotite and MORB samples and inferred for other planets. Melts are heavier than their mantle source regions to varying degrees based on redox state, degree of partial melting, and possibly other factors such as source mineralogy. Melting of isotopically light and possibly heterogeneous mantles in the Moon, Mars and Vesta gives rise to the observed range in basaltic compositions from those parent bodies.

References

Bourdon, B., Roskosz, M., Hin, R.C., 2018. Isotope tracers of core formation. Earth-Sci. Rev. 181, 61–81.

Cao, X., Bao, H., 2017. Redefining the utility of the three-isotope method. Geochim. Cosmochim. Acta 212, 16–32.

Craddock, P.R., Dauphas, N., 2011. Iron isotopic compositions of geological reference materials and chondrites. Geostand. Geoanal. Res. 35, 101–123.

Craddock, P.R., Warren, J.M., Dauphas, N., 2013. Abyssal peridotites reveal the near-chondritic Fe isotopic composition of the Earth. Earth Planet. Sci. Lett. 365, 63–76.

Dauphas, N., John, S.G., Rouxel, O., 2017. Iron isotope systematics. In: Teng, F.Z., Dauphas, N., Watkins, J.M. (Eds.), Non-Traditional Stable Isotopes. In: Reviews in Mineralogy and Geochemistry, vol. 82. Minerological Society of America, pp. 415–510. Ch. 11.

Dauphas, N., Roskosz, M., Alp, E.E., Neuville, D.R., Hu, M.Y., Sio, C.K., Tissot, F.L.H., Zhao, J., Tissandiere, L., Medard, E., Cordier, C., 2014. Magma redox and structural controls on iron isotope variations in Earth's mantle and crust. Earth Planet. Sci. Lett. 398, 127–140.

Dreibus, G., Wänke, H., 1980. The bulk composition of the eucrite parent asteroid and its bearing on planetary evolution. Z. Naturforsch. A, J. Phys. Sci. 35, 204–216.

Dreibus, G., Wänke, H., 1985. Mars, a volatile-rich planet. Meteoritics 20, 367–381. Hans Suess Festschrift.

Elardo, S.M., Draper, D.S., Shearer, C.K., 2011. Lunar Magma Ocean crystallization revisited: bulk composition, early cumulate mineralogy, and the source regions of the highlands Mg-suite. Geochim. Cosmochim. Acta 75, 3024–3045.

Elardo, S.M., Shahar, A., 2017. Non-chondritic iron isotope ratios in planetary mantles as a result of core formation. Nat. Geosci. 10, 317–321.

Halliday, A.N., Porcelli, D., 2001. In search of lost planets – the paleocosmochemistry of the inner solar system. Earth Planet. Sci. Lett. 192, 545–559.

Hansen, M., 1958. Constitution of Binary Alloys. Prepared with the cooperation of Kurt Anderko, 2nd ed. McGraw Hill.

Hin, R.C., Schmidt, M.W., Bourdon, B., 2012. Experimental evidence for the absence of iron isotope fractionation between metal and silicate liquids at 1 GPa and 1250–1300 °C and its cosmochemical consequences. Geochim. Cosmochim. Acta 93, 164–181.

Hume-Rothery, W., 1966. The Structures of Alloys of Iron: An Elementary Introduction. Pergamon Press.

Jordan, M.K., Tang, H.L., Kohl, I.E., Young, E.D., 2019. Iron isotope constraints on planetesimal core formation in the early solar system. Geochim. Cosmochim. Acta 246, 461–477.

Kato, C., Moynier, F., Valdes, M.C., Dhaliwal, J.K., Day, J.M.D., 2015. Extensive volatile loss during formation and differentiation of the Moon. Nat. Commun. 6.

Kono, Y., Kenney-Benson, C., Shibazaki, Y., Park, C., Shen, G.Y., Wang, Y.B., 2015. High-pressure viscosity of liquid Fe and FeS revisited by falling sphere viscometry using ultrafast X-ray imaging. Phys. Earth Planet. Inter. 241, 57–64.

Liu, J., Dauphas, N., Roskosz, M., Hu, M.Y., Yang, H., Bi, W.L., Zhao, J.Y., Alp, E.E., Hu, J.Y., Lin, J.F., 2017. Iron isotopic fractionation between silicate mantle and metallic core at high pressure. Nat. Commun. 8, 14337.

Lodders, K., Fegley, B., 1997. An oxygen isotope model for the composition of Mars. Icarus 126, 373–394.

Longhi, J., 1992. Experimental petrology and petrogenesis of mare volcanics. Geochim. Cosmochim. Acta 56, 2235–2251.

Longhi, J., 2006. Petrogenesis of picritic mare magmas: constraints on the extent of early lunar differentiation. Geochim. Cosmochim. Acta 70, 5919–5934.

Mandler, B.E., Elkins-Tanton, L.T., 2013. The origin of eucrites, diogenites, and olivine diogenites: magma ocean crystallization and shallow magma chamber processes on Vesta. Meteorit. Planet. Sci. 48, 2333–2349.

Mittlefehldt, D.W., 1987. Volatile degassing of basaltic achondrite parent bodies: evidence from alkali elements and phosphorus. Geochim. Cosmochim. Acta 51, 267–278.

Mittlefehldt, D.W., McCoy, T.J., Goodrich, C.A., Kracher, A., 1998. Non-chondritic meteorites from asteroidal bodies. In: Rev. Miner., vol. 36. Mineralogical Society of America, pp. 1–195. Ch. 4.

Musselwhite, D.S., Dalton, H.A., Kiefer, W., Treiman, A.H., 2006. Experimental petrology of the basaltic shergottite Yamato-980459: implications for the thermal structure of the Martian mantle. Meteorit. Planet. Sci. 41, 1271–1290.

O'Neill, H.S.C., 1991. The origin of the Moon and the early history of the Earth – a chemical model. Part 1: The Moon. Geochim. Cosmochim. Acta 55, 1135–1157.

O'Neill, H.S.C., Palme, H., 2008. Collisional erosion and the non-chondritic composition of the terrestrial planets. Philos. Trans. R. Soc., Math. Phys. Eng. Sci. 366, 4205–4238.

Papike, J.J., Fowler, G.W., Shearer, C.K., Layne, G.D., 1996. Ion microprobe investigation of plagioclase and orthopyroxene from lunar Mg-suite norites: implications for calculating parental melt REE concentrations and for assessing postcrystallization REE redistribution. Geochim. Cosmochim. Acta 60, 3967–3978.

Poitrasson, F., 2007. Does planetary differentiation really fractionate iron isotopes? Earth Planet. Sci. Lett. 256, 484–492.

Poitrasson, F., Delpech, G., Gregoire, M., 2013. On the iron isotope heterogeneity of lithospheric mantle xenoliths: implications for mantle metasomatism, the origin of basalts and the iron isotope composition of the Earth. Contrib. Mineral. Petrol. 165, 1243–1258.

Poitrasson, F., Halliday, A.N., Lee, D.C., Levasseur, S., Teutsch, N., 2004. Iron isotope differences between Earth, Moon, Mars and Vesta as possible records of contrasted accretion mechanisms. Earth Planet. Sci. Lett. 223, 253–266.

Poitrasson, F., Levasseur, S., Teutsch, N., 2005. Significance of iron isotope mineral fractionation in pallasites and iron meteorites for the core-mantle differentiation of terrestrial planets. Earth Planet. Sci. Lett. 234, 151–164.

Poitrasson, F., Roskosz, M., Corgne, A., 2009. No iron isotope fractionation between molten alloys and silicate melt to 2000 degrees C and 7.7 GPa: experimental evidence and implications for planetary differentiation and accretion. Earth Planet. Sci. Lett. 278, 376–385.

Pringle, E.A., Savage, P.S., Badro, J., Barrat, J.A., Moynier, F., 2013. Redox state during core formation on asteroid 4-Vesta. Earth Planet. Sci. Lett. 373, 75–82.

Righter, K., Chabot, N.L., 2011. Moderately and slightly siderophile element constraints on the depth and extent of melting in early Mars. Meteorit. Planet. Sci. 46, 157–176.

Righter, K., Drake, M.J., 1996. Core formation in Earth's Moon, Mars, and Vesta. Icarus 124, 513–529.

Righter, K., Drake, M.J., 1997. A magma ocean on Vesta: core formation and petrogenesis of eucrites and diogenites. Meteorit. Planet. Sci. 32, 929–944.

Russell, C.T., Raymond, C.A., Coradini, A., McSween, H.Y., Zuber, M.T., Nathues, A., De Sanctis, M.C., Jaumann, R., Konopliv, A.S., Preusker, F., Asmar, S.W., Park, R.S., Gaskell, R., Keller, H.U., Mottola, S., Roatsch, T., Scully, J.E.C., Smith, D.E., Tricarico, P., Toplis, M.J., Christensen, U.R., Feldman, W.C., Lawrence, D.J., McCoy, T.J., Prettyman, T.H., Reedy, R.C., Sykes, M.E., Titus, T.N., 2012. Dawn at Vesta: testing the protoplanetary paradigm. Science 336, 684–686.

Ruzicka, A., Snyder, G.A., Taylor, L.A., 1997. Vesta as the howardite, eucrite and diogenite parent body: implications for the size of a core and for large-scale differentiation. Meteorit. Planet. Sci. 32, 825–840.

Sanloup, C., Fiquet, G., Gregoryanz, E., Morard, G., Mezouar, M., 2004. Effect of Si on liquid Fe compressibility: implications for sound velocity in core materials. Geophys. Res. Lett. 31.

Sanloup, C., Guyot, F., Gillet, P., Fei, Y., 2002. Physical properties of liquid Fe alloys at high pressure and their bearings on the nature of metallic planetary cores. J. Geophys. Res., Solid Earth 107.

Sanloup, C., Guyot, F., Gillet, P., Fiquet, G., Hemley, R.J., Mezouar, M., Martinez, I., 2000. Structural changes in liquid Fe at high pressures and high temperatures from synchrotron X-ray diffraction. Europhys. Lett. 52, 151–157.

Schenk, T., Holland-Moritz, D., Simonet, V., Bellissent, R., Herlach, D.M., 2002. Icosahedral short-range order in deeply undercooled metallic melts. Phys. Rev. Lett. 89.

Schoenberg, R., von Blanckenburg, F., 2006. Modes of planetary-scale Fe isotope fractionation. Earth Planet. Sci. Lett. 252, 342–359.

Shahar, A., Elardo, S.M., Macris, C.A., 2017. Equilibrium fractionation of non-traditional stable isotopes: an experimental perspective. In: Rev. Mineral. Geochem., vol. 82. Mineralogical Society of America, pp. 65–83. Ch. 3.

Shahar, A., Hillgren, V.J., Horan, M.F., Mesa-Garcia, J., Kaufman, L.A., Mock, T.D., 2015. Sulfur-controlled iron isotope fractionation experiments of core formation in planetary bodies. Geochim. Cosmochim. Acta 150, 253–264.

Shahar, A., Schauble, E.A., Caracas, R., Gleason, A.E., Reagan, M.M., Xiao, Y., Shu, J., Mao, W., 2016. Pressure-dependent isotopic composition of iron alloys. Science 352, 580–582.

Shahar, A., Young, E.D., Manning, C.E., 2008. Equilibrium high-temperature Fe isotope fractionation between fayalite and magnetite: an experimental calibration. Earth Planet. Sci. Lett. 268, 330–338.

Shearer, C.K., Elardo, S.M., Petro, N.E., Borg, L.E., McCubbin, F.M., 2015. Origin of the lunar highlands Mg-suite: an integrated petrology, geochemistry, chronology, and remote sensing perspective. Am. Mineral. 100, 294–325.

Shibazaki, Y., Kono, Y., Fei, Y.W., 2015. Microscopic structural change in a liquid Fe–C alloy of similar to 5 GPa. Geophys. Res. Lett. 42, 5236–5242.

Sossi, P.A., 2017. A nickel for your planet's thoughts. Nat. Geosci. 10, 249–251.

Sossi, P.A., Moynier, F., 2017. Chemical and isotopic kinship of iron in the Earth and Moon deduced from the lunar Mg-suite. Earth Planet. Sci. Lett. 471, 125–135.

Sossi, P.A., Nebel, O., Anand, M., Poitrasson, F., 2016a. On the iron isotope composition of Mars and volatile depletion in the terrestrial planets. Earth Planet. Sci. Lett. 449, 360–371.

Sossi, P.A., Nebel, O., Foden, J., 2016b. Iron isotope systematics in planetary reservoirs. Earth Planet. Sci. Lett. 452, 295–308.

Steenstra, E.S., Knibbe, J.S., Rai, N., van Westrenen, W., 2016a. Constraints on core formation in Vesta from metal-silicate partitioning of siderophile elements. Geochim. Cosmochim. Acta 177, 48–61.

Steenstra, E.S., Rai, N., Knibbe, J.S., Lin, Y.H., van Westrenen, W., 2016b. New geochemical models of core formation in the Moon from metal-silicate partitioning of 15 siderophile elements. Earth Planet. Sci. Lett. 441, 1–9.

Stolper, E., 1977. Experimental petrology of eucritic meteorites. Geochim. Cosmochim. Acta 41, 587–611.

Teng, F.Z., Dauphas, N., Huang, S.C., Marty, B., 2013. Iron isotopic systematics of oceanic basalts. Geochim. Cosmochim. Acta 107, 12–26.

Wang, K., Jacobsen, S.B., Sedaghatpour, F., Chen, H., Korotev, R.L., 2015. The earliest Lunar Magma Ocean differentiation recorded in Fe isotopes. Earth Planet. Sci. Lett. 430, 202–208.

Wang, K., Moynier, F., Dauphas, N., Barrat, J.A., Craddock, P., Sio, C.K.I., 2012. Iron isotope fractionation in planetary crusts. Geochim. Cosmochim. Acta 89, 31–45.

Weber, R.C., Lin, P.-Y., Garnero, E.J., Williams, Q., Lognonne, P., 2011. Seismic detection of the lunar core. Science 331, 309–312.

Weyer, S., Anbar, A.D., Brey, G.P., Munker, C., Mezger, K., Woodland, A.B., 2005. Iron isotope fractionation during planetary differentiation. Earth Planet. Sci. Lett. 240, 251–264.

Weyer, S., Ionov, D.A., 2007. Partial melting and melt percolation in the mantle: the message from Fe isotopes. Earth Planet. Sci. Lett. 259, 119–133.

Weyer, S., Woodland, A., Munker, C., Arnold, G.L., Chakrabarti, R., Anbar, A.D., 2004. Iron isotope variations in the Earth's mantle and the terrestrial planets. Geochim. Cosmochim. Acta 68, A736.

Williams, H.M., Bizimis, M., 2014. Iron isotope tracing of mantle heterogeneity within the source regions of oceanic basalts. Earth Planet. Sci. Lett. 404, 396–407.

Williams, H.M., Markowski, A., Quitte, G., Halliday, A.N., Teutsch, N., Levasseur, S., 2006. Fe isotope fractionation in iron meteorites: new insights into metal-sulphide segregation and planetary accretion. Earth Planet. Sci. Lett. 250, 486–500.

Williams, H.M., Peslier, A.H., McCammon, C., Halliday, A.N., Levasseur, S., Teutsch, N., Burg, J.P., 2005. Systematic iron isotope variations in mantle rocks and minerals: the effects of partial melting and oxygen fugacity. Earth Planet. Sci. Lett. 235, 435–452.

Williams, H.M., Wood, B.J., Wade, J., Frost, D.J., Tuff, J., 2012. Isotopic evidence for internal oxidation of the Earth's mantle during accretion. Earth Planet. Sci. Lett. 321, 54–63.

Young, E.D., Manning, C.E., Schauble, E.A., Shahar, A., Macris, C.A., Lazar, C., Jordan, M., 2015. High-temperature equilibrium isotope fractionation of non-traditional stable isotopes: experiments, theory, and applications. Chem. Geol. 395, 176–195.

Zhao, X.M., Zhang, H.F., Zhu, X.K., Tang, S.H., Tang, Y.J., 2010. Iron isotope variations in spinel peridotite xenoliths from North China Craton: implications for mantle metasomatism. Contrib. Mineral. Petrol. 160, 1–14.